Applications of Polymer, Composite, and Coating Materials

Radio Frequency Heating of Carbon Nanotube Composite Materials

Charles Sweeney, Aaron Moran, Jacob Gruener, Alex Strasser, Martin Pospisil, Mohammad A. Saed, and Micah J. Green

ACS Appl. Mater. Interfaces, **Just Accepted Manuscript** • DOI: 10.1021/acsami.8b06268 • Publication Date (Web): 24 Jul 2018

Radio Frequency Heating of Carbon Nanotube Composite Materials

Charles B. Sweeney,[1] Aaron G. Moran,[2] Jacob T. Gruener,[2] Alex M. Strasser,[2] Martin J. Pospisil,[2] Mohammad A. Saed,[3] Micah J. Green[1,2*]

[1] Department of Materials Science & Engineering, Texas A&M University, College Station, TX, USA
[2] Artie McFerrin Department of Chemical Engineering, Texas A&M University, College Station, TX, USA
[3] Department of Electrical & Computer Engineering, Texas Tech University, Lubbock, TX, USA

*corresponding author: micah.green@tamu.edu, ORCID: 0000-0001-5691-0861

Abstract

Here, we give the first-ever report of RF electromagnetic heating of polymer nanocomposite materials via direct contact and capacitively-coupled electric field applicators. Notably, RF heating allows nanocomposite materials to be resistively heated with electric fields. We highlight our novel RF heating technique for multi-walled carbon nanotube (MWCNT) thermoplastic composites and measure their broadband dielectric properties. We also demonstrate three different electric field applicator configurations and discuss their practical use in an industrial setting. We demonstrate the use of RF heating to cure an automotive-grade epoxy loaded with MWCNTs. Our results show that lap shear joints cured faster with the RF method compared to control samples cured in an oven due to the heat transfer advantages of directly heating the epoxy composite. Finally, we implement our RF curing technique to assemble an automotive structure by locally curing an epoxy adhesive applied to a truck chassis.

Keywords: RF heating, nanotubes, nanomaterials, epoxy, thermoset, welding, composites

1. Introduction

Joule heating of nanocomposite materials has resulted in many unique applications for material processing, including embedded curing of composites, embedded heating elements for de-icing, and localized welding of 3D printed parts [1-3]. Most work to date has focused on direct current (DC) heating [4] or microwave heating of electrically conductive nanocomposite materials [5]. Radio frequency (RF) heating, defined by having an operating frequency from approximately 3 kHz to 300 MHz, is a largely unexplored method for heating of nanocomposite materials. Much of the historic use and research of RF heating has been focused on food processing [6-9], RF bonding or curing of materials [10,11], drying of raw materials [12], and biomedical hyperthermia or ablation [13-15]. Thermoset adhesives with high dielectric loss have been cured using high power RF energy [16]. To date, most of the literature has focused on RF heating of nanocomposites for hyperthermia applications [17-19], or inductively-coupled RF heating of nanocomposites [20,21]. (Note that induction heating is only efficient for materials with magnetic hysteresis losses, or with extraordinarily high

magnetic fields for conductive composites; in the case of CNT-loaded composites, induction heating is highly inefficient, and only works at short ranges when the material is placed inside the solenoid or just outside it. In contrast, RF heating with electric fields can operate over much larger distances and directly couples to the composite material.)

In comparison to DC or microwave heating, the benefits of capacitively-coupled RF heating include: (i) the flexibility to directly or remotely couple electromagnetic energy to a nanocomposite material, (ii) the ability to more efficiently transfer energy to the material due to capacitive coupling, (iii) the option to use sub-percolation loading levels of nanoparticle fillers, and (iv) reduction of safety concerns compared to microwaves by decreasing stray electromagnetic radiation [22].

Perhaps the simplest method for Joule heating a conductive nanocomposite material is to connect the composite to a direct current or line frequency (50-60 Hz) voltage source. Nearly all electric heating elements used in consumer or industrial applications operate in this manner. A notable example is the work from Lee and Wardle *et al.* who used DC heating to cure composite panels out-of-oven with embedded CNT films [23]. There are, however, two major draw-backs associated with DC Joule heating. First, the resistive material needs to be directly connected to the circuit with conductive electrodes, and second, the material needs to have a relatively high conductivity to pass a current through the material. High frequency alternating current (AC) electric fields may also be used to excite currents in conductive composite materials for heating applications. Microwave heating of CNT-loaded materials utilizes electromagnetic energy between 300 MHz and 300 GHz to heat lossy dielectrics and has the benefits of being able to remotely heat the target material with high energy density [24,25]; this rapid heating response is remarkable and has been used for a variety of applications. In our prior work, we demonstrated that the unique heating response of CNTs to microwaves can be used to rapidly weld 3D-printed thermoplastic structures together [3]. Even so, heating parts uniformly with microwaves is difficult, and shielding is required for preventing the emission of microwave energy that may be hazardous to humans or electronics [22]. There have no reports of CNTs showing similarly strong heating in the presence of lower frequency (MHz) fields.

Here we demonstrate a novel technique for heating nanocomposite materials with RF energy. We measure the RF electrical properties of CNT and polylactide (PLA) melt compounded nanocomposite films and evaluate various electric filled applicators for heating the films. We show that direct contact, parallel plate, and fringing field applicator geometries are all capable of heating nanotube composites at high heating rates. A practical example of curing a high strength epoxy loaded with CNTs in a lap shear joint configuration is shown. In this case, the aluminum lap shear coupons serve as the direct contact electrodes used to apply the RF energy to the epoxy nanocomposite. Due to the volumetric heating capability of the RF method, the RF-cured lap shear samples reached green strength in 3 minutes as opposed to 5 minutes for a conventional oven curing method. We anticipate wide applicability in the industrial manufacturing sector.

2. Results and Discussion

2.1 Electrical characterization

To fully understand the RF heating response of the polymer CNT composite materials, we first characterized hot pressed PLA films in the RF region using dielectric spectroscopy (**Figures S1-S2**). The dielectric properties are plotted as a function of frequency from 50 to 200 MHz in **Figures S3-S6**, along with the DC conductivity values measured using 4-point-probe (**Figure S7**). A large increase in conductivity is observed from 0.1 wt% to 0.5 wt% in both AC and DC data, indicating the onset of a percolated network. Note that the apparent AC conductivity at low loading levels is generally higher than DC conductivity. This is because of contributions from capacitive coupling of isolated CNTs, in contrast to DC percolation behavior where CNTs must be close enough to enable electron hopping or tunneling from CNT to CNT [26]. Note that nanomaterials other than CNTs may respond to RF fields, including graphene and carbon black, but the heating rates are substantially lower [27]. Prior reports have also established that the impurities that often accompany CNTs are not the primary source of heating.[28]

2.2 Thermographic spectroscopy

We heated the PLA/CNT composite films (0.5 mm thick) with RF power from 1 to 200 MHz and measured the heating rate as a function of frequency (**Figure 1, Figure S9-S15**). All samples from 0.1 wt% to 10 wt% efficiently couple to and heat in response to the applied RF energy. This result is surprising when compared with microwave heating of similar CNT composite films. In our prior study, we demonstrated that samples below 1 wt% heat very little in response to microwave energy, and samples above 5 wt% begin to reflect incident microwave energy and thus heat less [3]. The 5 wt% composite film achieved the highest heating rate of 16 ºC/s. All samples display heating rates that are highly dependent on frequency with notable resonant modes. Resonant modes common to at least two samples are centered at approximately 5 MHz, 35 MHz, 90 MHz, 120 MHz, and 180 MHz. As a general trend, the lower weight percent composite samples couple well at higher frequencies, and conversely, the higher weight percent composites couple at lower frequencies. This behavior is attributed to the fact that efficient coupling occurs at the frequencies where the impedance seen by the RF source (due to the sample, applicator, and connecting cables) and the impedance of the RF source are closely matched (complex conjugate of each other). Samples with lower CNT loadings have lower dielectric constants, and therefore, result in a lower capacitance for the RF applicator compared to samples with high CNT loadings since the capacitance is proportional to the dielectric constant. Lower capacitance means higher impedance since the impedance of a capacitor is inversely proportional to the capacitance. Consequently, the frequency at which efficient coupling occurs needs to be higher in order to lower the impedance to bring it closer to the source impedance. Furthermore, the resonant frequency of a resonant circuit is inversely proportional to the capacitance, lower capacitance (lower CNT loadings) results in a higher resonance frequency.

The two main factors that contribute to the observed resonant modes are the impedance of the composite films and the characteristics of RF amplifier circuit. The CNT composite samples

follow classic percolation models, and exhibit complex capacitive impedance, especially at lower loading levels. Based on the heating rate results in **Figure 1**, there exists a clear distinction between the film heating behavior above and below 2.5 wt%, with the 2.5 wt% sample exhibiting crossover behavior between the two responses. In our previous study with microwave heating, this bimodal response tracked well with the DC percolation threshold [3]. The higher-loading films have a higher density of resistive interconnects between carbon nanotubes dispersed in the matrix and behave more like an ideal resistor without a reactive component. The films with lower CNT loading are composed of a predominantly disjointed network of carbon nanotubes. Such a network may be represented by a combination of resistors and capacitors in series and parallel (**Figure 1 inset**). The greater the contribution from capacitive effects, the more sensitive the heating rate will be to the resonant frequency of the power supply and overall circuit. Note also that the precise locations of these peaks will vary based on CNT dispersion quality, which would alter the capacitive contributions. Note also that the addition of functional groups to the CNTs would improve dispersion quality but may also affect CNT-CNT contact resistance.[29]

2.3 RF circuit tuning and matching

Perhaps the most important consideration for effectively heating nanocomposite materials with RF energy is the concept of impedance matching [30-32]. Nanocomposite materials pose a unique challenge for matching, largely because their electrical properties can change over many orders of magnitude with small changes in composition or processing conditions. Additionally, nanocomposites are complex materials with both resistance and capacitance (the inductive component is negligible for non-magnetic nanocomposites). Maximum power is transferred from the RF source to the load when the equivalent load impedance Z_L (seen at the amplifier's output port) is equal to the complex conjugate of the RF source impedance Z_S^*, from the Thévenin equivalent circuit.

$$Z_L = Z_S^* \tag{1}$$

This implies that the real part of the impedances (the resistance R) must equal each other and the imaginary part of the impedances (the reactance X) must cancel,

$$Z = R + iX \tag{2}$$

$$R_S = R_L \tag{3}$$

$$X_S = -X_L \tag{4}$$

where R_S is the source resistance, R_L is the load resistance, X_S is the source reactance, and X_L is the load reactance. It is important to note that the load impedance includes both the sample impedance and the impedance of the cables and other circuit elements used to connect the

sample to the load; it is thus a lumped equivalent circuit. The complex impedance of the load Z_L may be defined as:

$$Z_L = R_L + iX_L = R_L + i\left(\omega L_L - \frac{1}{\omega C_L}\right) \quad (5)$$

where L_L is the inductance of the load, C_L is the capacitance of the load, and ω is the angular frequency given by $\omega = 2\pi f$. When the inductive and capacitive reactances are equal, the system is said to be at resonance. The resonance frequency ω_r of a series RLC circuit is given by:

$$\omega_r = 1/\sqrt{LC} \quad (6)$$

The RF source generally has a fixed resistance and zero reactance, and most commercial systems are designed to have an impedance of 50 Ohms. For our samples, the impedance is highly dependent on frequency, so these terms may be balanced to allow for efficient coupling by using frequency variation (as measured by heating rate in **Figure 1**). This could be used to employ RF-based curing of CNT/epoxy systems at low loadings, where samples with sub-percolation loadings may still strongly couple to fields with the appropriately matched resonant frequency.

In contrast, most industrial RF heating systems employ an operating frequency within one of the defined industrial, scientific, and medicine (ISM) bands designated for commercial use by the International Telecommunication Union (ITU) Radio Regulations (RR). Of the available bands, 13.56 MHz, 27.12 MHz, and 40.68 MHz are commonly used for heating [22]. In these cases, efficient heating could be accomplished through impedance matching, which is typically carried out with a matching network composed of variable inductor and capacitor elements either manually or automatically controlled.

Our system can be tailored based on composition of the nanocomposite rather than through the use of a matching network alone. This is also important because even matched systems that are as efficient as possible may be unable to heat a target material with low dielectric or resistive loss, i.e. an epoxy system that would normally require very high power levels to heat, could be made to heat at much lower power levels with the addition of a nanocomposite filler.

2.4 Applicator techniques

Demonstrations of both contact and non-contact RF heating were carried out on the composite films. The direct contact method is the same as that used for the thermographic spectroscopy technique. Silver electrodes were painted onto the edges of the composite films and connected to the RF amplifier with alligator clips; one electrode is grounded and the other carries the sinusoidal RF signal (**Figure 2A**). For the non-contact methods, we utilize the electric fields produced between the ground and RF signal lines to induce a time-varying electric field in the

composite films resulting in resistive heating. We demonstrate both a parallel plate capacitor-like arrangement (**Figure 2B**), and a planar interdigitated fringing-field applicator (**Figure 2C**). The parallel plate system consists of two copper discs approximately 5 cm in diameter fixed to an insulating support bar. One disc is grounded, while the other is connected to the center pin of the coaxial cable from the RF power source. Samples are placed in-between the discs without physically touching either electrode. For the fringing field applicator, copper tape 5 mm in width was laid down on a polyetherimide sheet to create a pattern of interdigitated "fingers." The copper was covered with an insulating layer of Kapton tape and soldered to the ground and center pin of a Type N bulkhead connector. Thin composite samples were heated by placing them parallel to the interdigitated applicator within approximately 5 mm from the surface of the applicator.

In all three cases, the samples heat rapidly in response to the applied electric field (**SI Movies S1, 2, 3 and 4**) with heating rates over 100˚C/s observed in response to power levels of a few hundred watts. The direct contact configuration in **Figure 2D** shows the heat generated in a 1.0 wt% CNT PLA film at 315 W applied power at 100 MHz after 4 seconds of applied power. This is the simplest RF field application method and was generally least sensitive to factors such as film orientation in the electric field. The non-contact heating results are similarly energetic. We used a 7.5 wt% CNT PLA film and applied 100 W of power at 100 MHz; **Figure 2E** shows the heat generated in the film after 6 seconds. This applicator configuration would be very useful for targeted heating of a material that is embedded or otherwise inaccessible to directly contact with metallic electrodes. Another useful application could be the efficient and direct heating of a nanocomposite material in a tube furnace where indirect heating via an oven is typically implemented.

Finally we show an interdigitated fringing field applicator heating a 1.0 wt% CNT PLA film at 315 W applied power at 50 MHz and the intense heat generated after 1 second (**Figure 2F**). The interdigitated fringing field applicator has a serpentine electric field shape (**Figure S16-18**). In **Fig. 2F**, the portion of the PLA film covering the field lines heats up leading to a similar thermal pattern in the PLA film. Such a fringing field applicator is specifically useful for heating planar materials moving in reference to each other (either the material moves relative to the fringing field applicator or vice versa). The act of scanning the fringing field parallel to the field lines serves to uniformly heat the sheet or film. This configuration may find uses in heat treating nanocomposite thin films, thermographically characterizing the electrical properties of printed electronics, and processing continuous feeds of materials.

Both non-contact methods are operated in an "electrically small" configuration, i.e., the dimensions of the applicator are less than one-eighth the wavelength of the applied RF field (at 200 MHz the wavelength is approximately 1.5 m) [22]. Because of this, the electric fields generated between the plates or interdigitated fingers cannot establish standing waves, and so are highly uniform in nature. Note that each of these applicators would have slightly different frequency-dependent reactance and shift the heating rate results seen in **Figure 1**.

2.5 COMSOL modeling

The applicator configurations above were modeled in COMSOL to develop a better understanding of the electric field distribution in the samples and the coupled heat generated by the RF energy. Modeling the applicator geometry and sample to be heated can be a valuable tool for creating an efficient and effective RF heating module in a real-world application. For this geometry, we modeled the electric field with a lumped port, and assume a power input of 100 W; for a 50 Ohm system, this results in a peak voltage input of 100V. The dielectric properties of the film were taken from the measurements we performed earlier. Using COMSOL Multiphysics RF and Heat Transfer modules, we calculated the electric field distribution in the film and coupled that with the material dielectric properties to determine the power dissipation and thus the temperature rise in the material. We show in **Figure 3** the electric field distribution (left), the temperature rise (middle), and power dissipation density (right) for a capacitively-coupled parallel plate applicator (SI Movie 5). Calculating the maximum predicted electric field strength is important to ensure that the system is operated well below the dielectric breakdown voltage of air (approximately 3 MV/m) and the breakdown strength of the composite materials to be heated. Outside the sample, the maximum electric field concentrates around the sharp edges of the applicator plates and the corners of the sample. Note that the strong electric field intensity shown in **Figure 3** (left) is in the air gap region between the plates and the sample. (The same simulation is shown without the sample in **Figure S19**.) This is due to the fact that for the parallel plate configuration considered in this simulation, the electric field is almost perpendicular to the interface between the air region and the sample. Boundary conditions for the electromagnetic fields dictate that the normal component of the electric flux density $\vec{D}$ must be continuous across the interface between the air region and the dielectric region (the sample). The electric flux intensity $\vec{E}$ is related to the electric flux density $\vec{D}$ through the relation $\vec{E} = \vec{D}/\epsilon$ where ϵ is the material's permittivity. For and ideal parallel plate configuration, $\vec{D}$ is the same in both regions, consequently, the electric field intensity $\vec{E}$ in the air gap region is stronger than in the dielectric sample since the permittivity of the dielectric is higher than that of air. Within the dielectric sample, more heating occurs in the sample's center, as shown in **Figure 3** (middle), which is consistent with power dissipation in **Figure 3** (right). Heating is due to induced currents in the sample, power dissipated in the sample (as heat) is proportional to the induced currents. The current distribution within the sample is maximum at the sample's center and gradually drops towards the edges near the plates. However, the electric field and the heating across various samples is more uniform than the results we previously showed for microwave waveguide heating of composite films where heating uniformity was highly dependent on the dielectric properties of the film [3,33].

2.6 Application to rapid bonding

We now demonstrate an automotive- and aerospace-focused application of this technology by bonding aluminum sheets with a high performance epoxy adhesive loaded with multi-walled carbon nanotubes (SI Movie 6). It is highly desirable to bond aluminum and composite parts with high-performance adhesives instead of rivets or traditional welds [34-36]. Properly selected adhesives outperform both welds and mechanical fasteners in regard to mechanical strength, impact and fatigue resistance as well as weight. Historically, the one-part epoxies used to bond

vehicle components required cure temperatures of 180˚C for 30 minutes to reach full strength [37]. This required the components to be placed in large ovens, draped with heater blankets, hot air guns, or infrared heaters to achieve the desired degree of cure. With our RF curing technique, the epoxy adhesive composite volumetrically generates the required heat for curing because of Joule heating of the embedded CNTs. We prepared samples of a one-part automotive grade epoxy system (Dow Betamate™) loaded with 0.25 wt% CNTs, which is below the classical DC percolation threshold, and yet still couples effectively with the RF power source. Lap shear samples were connected to the RF source (**Figure 4A**) and monitored with a FLIR camera so that power could be manually controlled to achieve a desired thermal cure profile (**Figure 4B**). The samples all had an initial heating rate of approximately 5˚C/s, similar to the direct-contact hot pressed films shown in the previous section. The heating rate is determined by the applied RF power minus heat flux to the components being joined. The maximum heating rate is governed by the dielectric breakdown strength of the epoxy CNT composite, the degradation temperature of the epoxy, or other thermal considerations for the components to be joined. At higher loading levels (>0.5 wt.%) we did in fact observe dielectric breakdown and arcing events if the power level (and thus the electric field) was raised too high. Using low CNT filler loading levels, an adhesive with higher dielectric breakdown strength, or more sophisticated RF equipment may all help to mitigate breakdown events.

Our RF curing method allowed the sample to be brought up to the desired cure temperature of 200˚C within 2 minutes by applying up to 100 Watts of RF power at 44 MHz. After 3 minutes of heating, the RF-cured sample passed a green strength test, holding an 8.2 kg mass for a minimum of 30 seconds; the sample continued to hold the weight for 30 minutes before we removed the grips (**Figures S20-S26**). The remaining RF lap shear samples cured for 4 and 5 minutes each passed the green strength test (**Figure 4C**). In contrast, the control samples (cured via convective heat transfer in an oven set to 200˚C) took 5 minutes to cure to green strength. After 4 minutes, the lap shear sample had begun to cure; however the sample slipped via adhesive failure after a few seconds of the grips and weight being applied.

This difference between the RF curing and oven curing process is best explained by the heat transfer mechanisms at work. In the RF curing technique, heat is generated volumetrically within the adhesive system itself via capacitively-coupled Joule heating of the sub-percolated CNT network. In the oven curing technique, the limiting factor is the convective heat transfer to the aluminum strips *and* the conduction heating into the epoxy. Epoxies, as well as most adhesive systems, are poor thermal conductors and share the same rate limiting steps governed by Fourier's law. Especially in the automotive manufacturing sector where cycle times dictate which technologies are production-ready, volumetric RF curing of nanocomposite epoxies offers excellent opportunities for rapid curing of adhesive joints. Furthermore, volumetric curing would allow for spatially-uniform cure state over large samples [38-41].

Besides using less active filler material, the low loading levels of CNTs ensure the adhesive maintains its inherent mechanical properties, and is not significantly embrittled. This is also advantageous from a cost perspective by limiting the amount of nanomaterial filler necessary to achieve sufficient heating performance. Additional advantages for industrial applications include

a large reduction in capital equipment costs typically associated with large ovens, custom tooling, and other heating elements. This heating method is highly efficient from an energy perspective since heat is generated directly within the target material; similar to induction heating, excessive heat losses are thus minimized [42].

In **Figure 5** (and **Figures S27-30** and **SI Movie 7**), we show an example of a model truck being bonded together with the RF technique we developed. The truck bed was removed with a metal cut-off wheel (**Figure 5B**) and prepared with the CNT-loaded Betamate™ epoxy. We grounded the truck body and connected the truck bed to be bonded to the hot side of the RF source (**Figure 5C**). After a few minutes of heating, the truck was fully bonded together to its green strength (**Figure S29**) and was able to support a 1.4 kg load in the truck bed (**Figure 5D and S30**). It is clear from the FLIR images that heat emanates locally from the composite epoxy, this allowed the plastic components to be left on the model without melting them (this would not be possible with curing in an oven at 200˚C). Such a technique may be applied on a full scale vehicle production line with robotic assembly equipment. Certain parts of the vehicle to be bonded could be connected to an RF power supply while the rest of the body is grounded. This would eliminate costly tooling, IR heaters, induction heaters, or ovens conventionally used to cure these epoxy bonds. Instead the components to be bonded are the electrodes and part of the circuit used to bond the heat-generating epoxy composite.

3. Conclusion

We highlight the advantages of RF heating and demonstrate for the first time the use of RF energy to heat polymer nanocomposites. By characterizing the dielectric properties of the material we are able to understand the mechanism for RF heating of the CNT composite materials used in this study. Various electric field applicator configurations including direct contact, parallel plate, and interdigitated fringing field applicators have been demonstrated by heating PLA/CNT composite films. We also have highlighted the practical use of this technique for bonding epoxy lap shear samples, and show that RF heating was able to achieve green strength two minutes faster than an oven-cured counterpart.

Associated Content: Supporting Information

The Supporting Information is available free of charge on the ACS Publications website at DOI: _____

Additional experimental heating data as well as RF applicator and mechanical testing images.

Notes: The technology described in this manuscript is covered by a Texas A&M patent with C.B. Sweeney, M.A. Saed, and M.J. Green as co-authors.

Acknowledgements

We acknowledge helpful advice from J. Harris of TAMU; F. Mirri, M. Pasquali of Rice; R. Vano, B. Zahner, B. Teipel, E. Teipel of Essentium Materials, T. Auvil, D. Sophiea of Dow. This

material is based upon work supported by the U.S. National Science Foundation (CMMI-1561988) and by the U. S. Army Research Office under contract/grant W911NF-15-1-0039.

Experimental Section

Sample preparation

Carbon nanotube polylactide (PLA) composite films (**Figure S1**) were prepared via melt compounding. Starting with a 10.0 wt% MWCNT/PLA masterbatch (Nanocyl SA, custom batch, Catalytic Chemical Vapor Deposition process used for MWCNT growth), various dilutions were melt compounded into neat PLA (NatureWorks LLC, 3D850) with a micro-conical twin screw compounder (Thermo Fisher Scientific Inc., HAAKE™ MiniCTW). Prior to compounding, the polymer samples were thoroughly dried per the manufacturer's specifications. Samples were melt compounded for approximately 4 minutes at 215 ºC before the die was opened and the sample allowed to extrude. The nanocomposite dilutions were then hot-pressed (Carver Inc., model 3856) into uniform 0.5 mm thick films at 150 ºC and 27.6 MPa. Rectangular samples 3 x 5 cm were cut from the films and silver electrodes were painted onto the edges to aid in contact to the RF applicator cables.

Impedance spectrometry

The complex permittivity was measured using a capacitive sample holder consisting of two conducting cylindrical disks (**Figure S2**) and a network analyzer. An adapter was used to convert N-type coaxial connection from the network analyzer to two parallel prongs to connect to the capacitor disks. In the measurement, the sample under test is placed between the two disks and the scattering parameter S_{11} is acquired for the desired frequency range. A calibration procedure was used to account for the connecting cables and the adapter and capacitor parasitics. The capacitor impedance is obtained from the measured S_{11} parameter, which is then used to compute the complex permittivity, taking into account the fringing fields.

Thermographic spectroscopy

Radio frequency power was applied to the samples with a signal generator (Rigol Inc., DSG815) and 500 W amplifier (Prana R&D, GN500D). The samples were connected to the amplifier with a 50 Ω coaxial transmission line terminated by a Type N bulkhead connector with alligator clips soldered to the center pin and ground reference. Samples were placed in a custom laminar airflow box to have a consistent advective cooling rate across all samples. The samples were directly monitored with a FLIR infrared camera system (FLIR Systems Inc., A655sc). To test the frequency dependent heating response of the samples and the RF power equipment, a step-wise heat-cool frequency sweep was programmed into the signal generator. Frequencies from 1-200 MHz were swept such that power at 40 dBm (10 W) is applied for 2 seconds, followed by 13 seconds of cooling before moving to the next 1 MHz incremental step. The heating rates as a function of frequency were determined by selecting the points when the power is switched on and 1 second into each cycle and calculating the slope between the points as shown in **Figure**

S8. The complete datasets for each sample are shown in **Figures S6-S12**. (Note, additional images of applicators shown in Figures S13-15.)

Lap shear RF bonding

Aluminum strips (ThyssenKrupp Materials NA Inc., 7075 T6) 1mm thick and 25.4 mm wide by 152.4 mm long were bonded using a single-part high temperature cure epoxy (Betamate™, DowDuPont Inc.) loaded with MWCNTs (Cheap Tubes Inc.). The epoxy and CNT's (0.25 wt%) were mixed with a planetary centrifugal mixer (AR-100, THINKY USA, Inc.) at 2000 RPM for 15 minutes. Lap shear samples were prepared and tested for lap shear strength according to ASTM D1002 (**Figure S16**). Polyetherimide (PEI) spacers were inserted on both edges of the lap shear samples to ensure a consistent bond line thickness was maintained for every sample. A strip of Kapton polyimide (PI) tape was used to clamp the strips in position during the curing procedure (**Figure S16**). Control samples were cured in an oven according to the manufactures recommended processing conditions. The samples were suspended across thermally insulating alumina bricks to ensure convention heating dominated rather than thermal conduction through the aluminum strips (**Figure S17**). The oven was pre-heated to 200˚C and samples were timed according to the total residence time in the oven, ranging from 2-6 minutes. For the RF cured samples, the prepared specimens were connected to the RF amplifier (**Figure S18**) by grounding one of the aluminum strips and connecting the other to the center pin of the Type N bulkhead connector. The applied power was approximately 10-100 W at 44 MHz throughout the curing process and was manually controlled by directly observing the temperature of the samples with a FLIR camera (**Figure S19**). The "green strength" of the joint was assessed by curing the specimen at a specified time at 200˚C, followed by immediately weighting the lap shear specimen with 8.2 kg (**Figure S20**). Samples that could hold the weight without measureable joint displacement were defined as having reached their green strength, conversely, if the lap shear joint failed, the specimen was defined as failing the green strength.

References

(1) Odom, M. G. B.; Sweeney, C. B.; Parviz, D.; Sill, L. P.; Saed, M. A.; Green, M. J. Rapid Using and Additive Manufacturing of Thermoset Systems Using Scanning Microwave Heating of Carbon Nanotube/Epoxy Composites. *Carbon* **2017**, *120*, 447-453.

(2) Janas, D.; Koziol, K. K. Rapid Electrothermal Response of High-temperature Carbon Nanotube Film Heaters. *Carbon* **2013**, *59*, 457-463.

(3) Sweeney, C. B.; Lackey, B. A.; Pospisil, M. J.; Achee, T. C.; Hicks, V. K.; Moran, A. G.; Teipel, B. R.; Saed, M. A.; Green, M. J. Welding of 3d-printed Carbon Nanotube-polymer Composites by Locally Induced Microwave Heating. *Sci. Adv.* **2017**, *3*.

(4) Koerner, H.; Price, G.; Pearce, N. A.; Alexander, M.; Vaia, R. A. Remotely Actuated Polymer Nanocomposites - Stress-recovery of Carbon-nanotube-filled Thermoplastic Elastomers. *Nat. Mater.* **2004**, *3*, 115-120.

(5) Zhang, M.; Fang, S. L.; Zakhidov, A. A.; Lee, S. B.; Aliev, A. E.; Williams, C. D.; Atkinson, K. R.; Baughman, R. H. Strong, Transparent, Multifunctional, Carbon Nanotube Sheets. *Science* **2005**, *309*, 1215-1219.

(6) Marra, F.; Zhang, L.; Lyng, J. G. Radio Frequency Treatment of Foods: Review of Recent Advances. *J. Food Eng.* **2009**, *91*, 497-508.

(7) Orsat, V.; Raghavan, G. S. V. Radio-Frequency Processing. *Emerging Technologies for Food Processing* **2005**, 445-468.

(8) Piyasena, P.; Dussault, C.; Koutchma, T.; Ramaswamy, H. S.; Awuah, G. B. Radio Frequency Heating of Foods: Principles, Applications and Related Properties - a Review. *Crit. Rev. Food Sci. Nutr.* **2003**, *43*, 587-606.

(9) Zhao, Y. Y.; Flugstad, B.; Kolbe, E.; Park, J. W.; Wells, J. H. Using Capacitive (Radio Frequency) Dielectric Heating in Food Processing and Preservation - a Review. *J. Food Process Eng.* **2000**, *23*, 25-55.

(10) Sano, M.; Oguma, H.; Sekine, M.; Sekiguchi, Y.; Sato, C. High-frequency Welding of Glass-fibre-reinforced Polypropylene with a Thermoplastic Adhesive Layer: Effects of Ceramic Type and Long-term Exposure on Lap Shear Strength. *Int. J. Adhes. Adhes.* **2015**, *59*, 7-13.

(11) Leighton, J.; Brantley, T.; Szabo, E. RF Welding of Pvc and Other Thermoplastic Compounds. *J. Vinyl Addit. Technol.* **1993**, *15*, 188-192.

(12) Avramidis, S.; Zwick, R. L. Exploratory Radio-frequency/Vacuum Drying of Three Bc Coastal Softwoods. *For. Prod. J. (USA)* **1992**.

(13) Gazelle, G. S.; Goldberg, S. N.; Solbiati, L.; Livraghi, T. Tumor Ablation with Radio-frequency Energy. *Radiology* **2000**, *217*, 633-646.

(14) Goldberg, S. N.; Ahmed, M.; Gazelle, G. S.; Kruskal, J. B.; Huertas, J. C.; Halpern, E. F.; Oliver, B. S.; Lenkinski, R. E. Radio-frequency Thermal Ablation with Nacl Solution Injection: Effect of Electrical Conductivity on Tissue Heating and Coagulation-phantom and Porcine Liver Study. *Radiology* **2001**, *219*, 157-165.

(15) Pavlovich, C. P.; Walther, M. M.; Choyke, P. L.; Pautler, S. E.; Chang, R.; Linehan, W. M.; Wood, B. J. Percutaneous Radio Frequency Ablation of Small Renal Tumors: Initial Results. *J. Urol.* **2002**, *167*, 10-15.

(16) Li, C.; Dickie, R. A. Bonding Adhesive Joints with Radiofrequency Dielectric Heating. *Int. J. Adhes. Adhes.* **1991**, *11*, 241-246.

(17) Gannon, C. J.; Cherukuri, P.; Yakobson, B. I.; Cognet, L.; Kanzius, J. S.; Kittrell, C.; Weisman, R. B.; Pasquali, M.; Schmidt, H. K.; Smalley, R. E.; Curley, S. A. Carbon Nanotube-enhanced Thermal Destruction of Cancer Cells in a Noninvasive Radiofrequency Field *Cancer* **2007**, *110*, 2654-2665.

(18) Corr, S. J.; Raoof, M.; Cisneros, B. T.; Orbaek, A. W.; Cheney, M. A.; Law, J. J.; Lara, N. C.; Barron, A. R.; Wilson, L. J.; Curley, S. A. Radiofrequency Electric-field Heating Behaviors of Highly Enriched Semiconducting and Metallic Single-walled Carbon Nanotubes. *Nano Res.* **2015**, *8*, 2859-2870.

(19) Lara, N. C.; Haider, A. A.; Ho, J. C.; Wilson, L. J.; Barron, A. R.; Curley, S. A.; Corr, S. J. Water-structuring Molecules and Nanomaterials Enhance Radiofrequency Heating in Biologically Relevant Solutions. *Chem. Commun. (Cambridge, U.K.)* **2016**, *52*, 12630-12633.

(20) Satarkar, N. S.; Johnson, D.; Marrs, B.; Andrews, R.; Poh, C.; Gharaibeh, B.; Saito, K.; Anderson, K. W.; Hilt, J. Z. Hydrogel-mwcnt Nanocomposites: Synthesis, Characterization, and Heating with Radiofrequency Fields. *J. Appl. Polym. Sci.* **2010**, *117*, 1813-1819.

(21) He, Z. W.; Satarkar, N.; Xie, T.; Cheng, Y. T.; Hilt, J. Z. Remote Controlled Multishape Polymer Nanocomposites with Selective Radiofrequency Actuations. *Adv. Mater.* **2011**, *23*, 3192-+.

(22) Mehdizadeh, M.: *Microwave/RF Applicators and Probes: For Material Heating, Sensing, and Plasma Generation*; William Andrew, 2015.

(23) Lee, J.; Stein, I. Y.; Kessler, S. S.; Wardle, B. L. Aligned Carbon Nanotube Film Enables Thermally Induced State Transformations in Layered Polymeric Materials. *ACS Appl. Mater. Interfaces* **2015**, *7*, 8900-8905.

(24) Qin, F.; Brosseau, C. A Review and Analysis of Microwave Absorption in Polymer Composites Filled with Carbonaceous Particles. *J. Appl. Phys. (Melville, NY, U. S.)* **2012**, *111*, 24.

(25) Menendez, J. A.; Arenillas, A.; Fidalgo, B.; Fernandez, Y.; Zubizarreta, L.; Calvo, E. G.; Bermudez, J. M. Microwave Heating Processes Involving Carbon Materials. *Fuel Process. Technol.* **2010**, *91*, 1-8.

(26) Gau, C.; Kuo, C.-Y.; Ko, H. Electron Tunneling in Carbon Nanotube Composites. *Nanotechnology* **2009**, *20*, 395705.

(27) Irin, F.; Shrestha, B.; Cañas, J. E.; Saed, M. A.; Green, M. J. Detection of Carbon Nanotubes in Biological Samples Through Microwave-induced Heating. *Carbon* **2012**, *50*, 4441-4449.

(28) Vázquez, E.; Prato, M. Carbon Nanotubes and Microwaves: Interactions, Responses, and Applications. *ACS Nano* **2009**, *3*, 3819-3824.

(29) Grady, B. P.: *Carbon Nanotube - Polymer Composites Heating*; Wiley: Hoboken, N.J., 2011.

(30) Neophytou, R. I.; Metaxas, A. C. Characterisation of Radio Frequency Heating Systems in Industry Using a Network Analyser. *IEE Proc.: Sci., Meas. Technol.* **1997**, *144*, 215-222.

(31) Neophytou, R. I.; Metaxas, A. C. Combined Tank and Applicator Design of Radio Frequency Heating Systems. *IEE Proc., Part H: Microwaves, Opt. Antennas* **1999**, *146*, 311-318.

(32) Neophytou, R. I.; Metaxas, A. C. Determination of Resonant Modes of Rf Heating Systems Using Eigenvalue Analysis. *J. Microwave Power* **2000**, *35*, 3-14.

(33) Haile, M.; Sweeney, C. B.; Lackey, B. A.; Sarwar, O.; Henderson, R.; Saed, M. A.; Green, M. J.; Grunlan, J. C. Ultrafast and Highly Localized Microwave Heating in Carbon Nanotube Multilayer Thin Films. *Adv. Mater. Interfaces* **2017**, *4*, 6.

(34) Messler, R. W.: *Joining of Materials and Structures: From Pragmatic Process to Enabling Technology*; Butterworth-Heinemann, 2004.

(35) Alfano, M.; Furgiuele, F.; Pagnotta, L.; Paulino, G. H. Analysis of Fracture in Aluminum Joints Bonded with a Bi-component Epoxy Adhesive. *J. Test. Eval.* **2011**, *39*, 296-303.

(36) Kinloch, A. J.: *Adhesion and Adhesives: Science and Technology;* Springer Science & Business Media, 2012.

(37) Joining Technologies. *pro Active,* December, 2004.

(38) Chang, J.; Liang, G.; Gu, A.; Cai, S.; Yuan, L. The Production of Carbon Nanotube/Epoxy Composites with a Very High Dielectric Constant and Low Dielectric Loss by Microwave Curing. *Carbon* **2012**, *50*, 689-698.

(39) Sung, P.-C.; Chiu, T.-H.; Chang, S.-C. Microwave Curing of Carbon Nanotube/Epoxy Adhesives. *Compos. Sci. Technol.* **2014**, *104*, 97-103.

(40) Fotiou, I.; Baltopoulos, A.; Vavouliotis, A.; Kostopoulos, V. Microwave Curing of Epoxy Polymers Reinforced with Carbon Nanotubes. *J. Appl. Polym. Sci.* **2013**, *129*, 2754-2764.

(41) Odom, M. G.; Sweeney, C. B.; Parviz, D.; Sill, L. P.; Saed, M. A.; Green, M. J. Rapid Curing and Additive Manufacturing of Thermoset Systems Using Scanning Microwave Heating of Carbon Nanotube/Epoxy Composites. *Carbon* **2017**, *120*, 447-453.

(42) Rudnev, V.; Loveless, D.; Cook, R. L.: *Handbook of Induction Heating*; CRC Press, 2017.

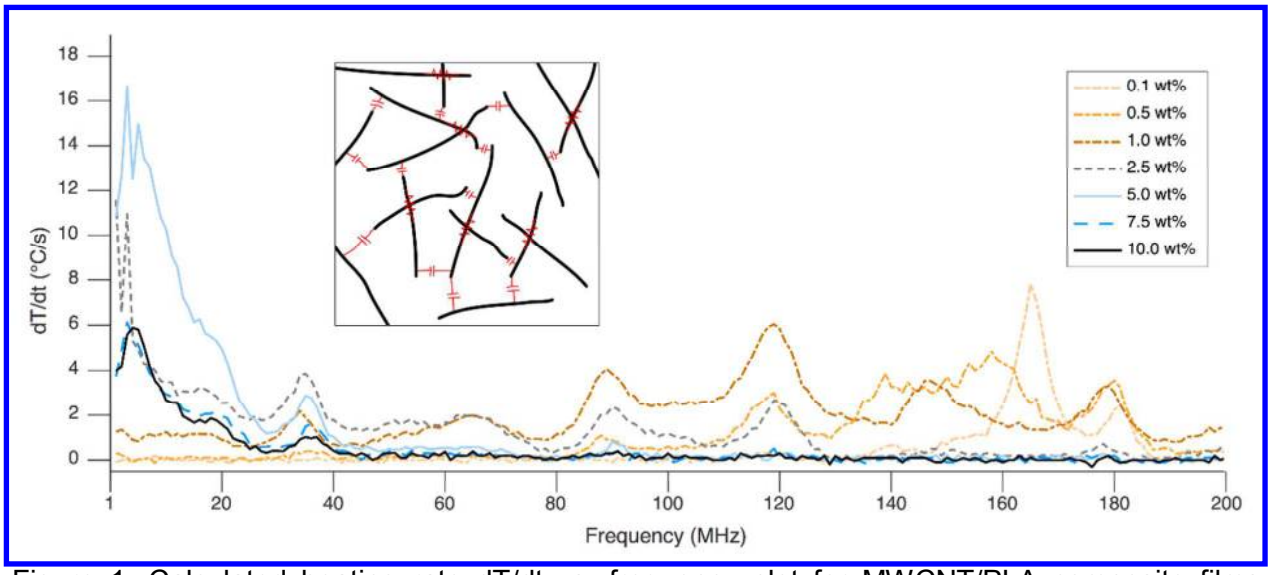

Figure 1. Calculated heating rate dT/dt vs. frequency plot for MWCNT/PLA composite films heated via direct-contact RF energy (inset: RC CNT network illustration).

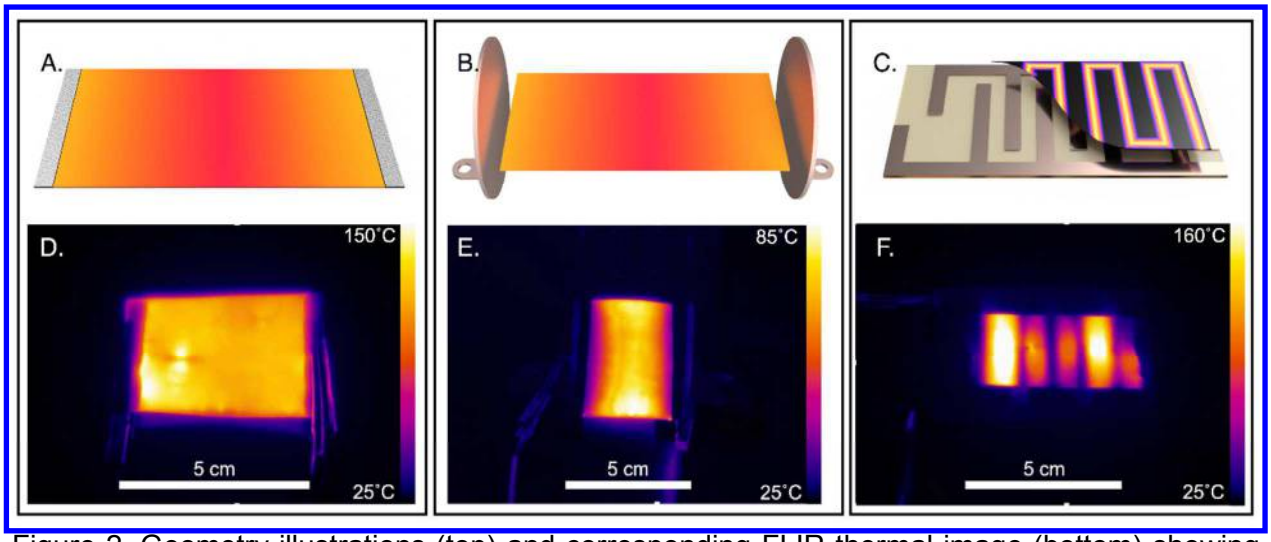

Figure 2. Geometry illustrations (top) and corresponding FLIR thermal image (bottom) showing the three RF electric field applicator configurations: direct contact (A) parallel plate (B) and interdigitated fringing field (C). These three applicators are applied to three samples: (D) 1.0 wt% MWCNT in PLA at 315 W, 100 MHz, 4 seconds; (E) 7.5 wt% MWCNT in PLA at 100 W, 100 MHz, 6 seconds; (F) 1.0 wt% MWCNT in PLA at 315 W, 50 MHz, 1 second.

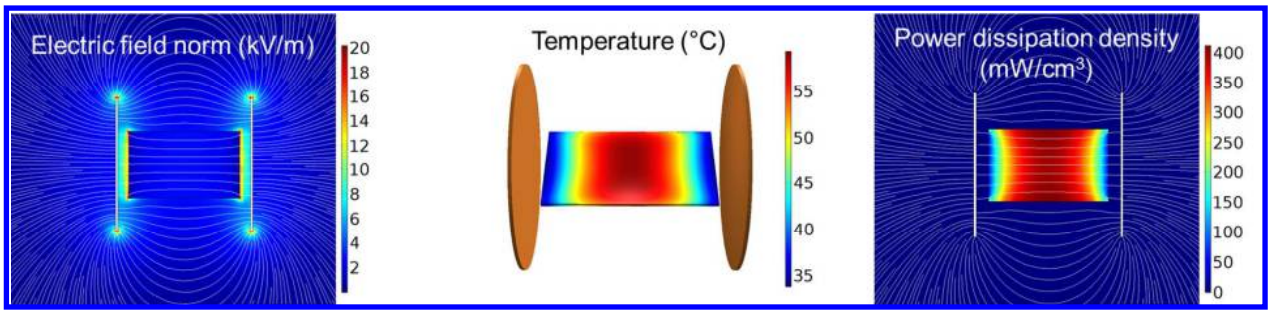

Figure 3. COMSOL models showing electric field strength around the sample (2.5wt% CNT in PLA) and near the electrodes (left) the steady state temperature field generated in a sample (middle) and the power dissipation density (right).

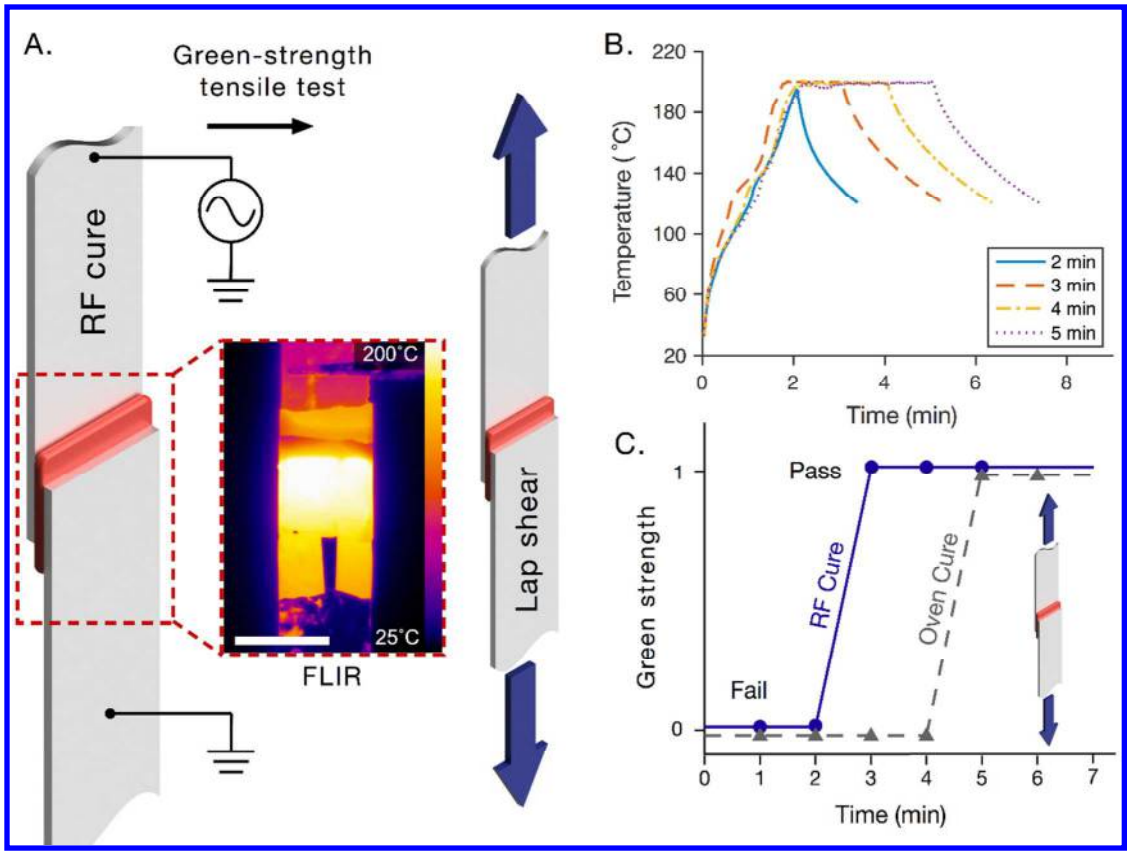

Figure 4. (A) Lap shear strength sample geometry showing the RF applicator technique, and the thermal profile recorded with a FLIR thermal camera (scalebar = 1 inch). (B) Temperature profile as a function of RF cure time recorded by the FLIR camera. (C) Time to reach equivalent green strength for traditional oven cure and RF curing technique.

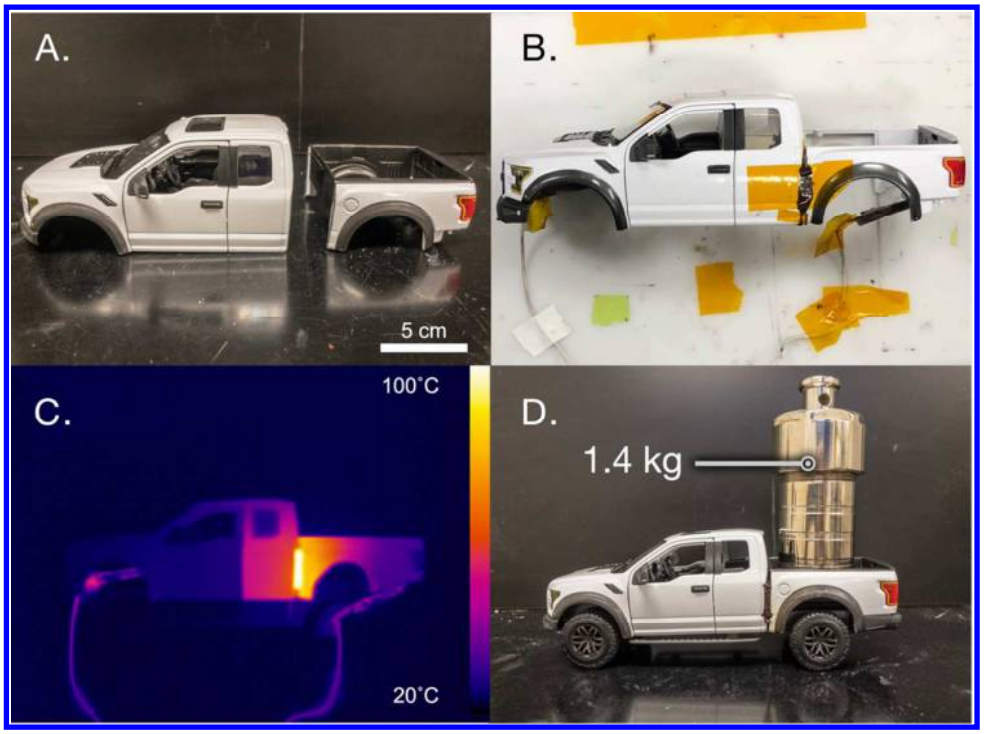

Figure 5. A model truck (A) was bisected by cutting the truck bed off. (B) The truck and bed interface was filled with CNT loaded Betamate™ epoxy and connected to the RF source. (C) The interface containing the epoxy rapidly heated and the temperature was monitored with the FLIR camera. (D) The finished, welded truck was able to support weight (1.4 kg) in the truck bed.

TOC image